The electronic, vibrational and dielectric properties of diamond crystals with neutral vacancies: first principles study

L.L. Rusevich [a,*], E.A. Kotomin [a,b,**], A.I. Popov [a], G. Aiello [c], T.A. Scherer [c], A. Lushchik [d]

[a] Institute of Solid State Physics, University of Latvia, 8 Kengaraga Str., LV-1063, Riga, Latvia
[b] Max Planck Institute for Solid State Research, Heisenberg Str. 1, 70569, Stuttgart, Germany
[c] Karlsruhe Institute of Technology, Hermann-von-Helmholtz-Platz 1, D-76344, Eggenstein-Leopoldshafen, Germany
[d] Institute of Physics, University of Tartu, 1 W. Ostwald Str., 50411, Tartu, Estonia

Keywords:
Diamond
Vacancy
Electronic structure
Spin state
Dielectric properties
First principles calculations

A B S T R A C T

The atomic and electronic structure as well as vibrational and dielectric properties (including first calculations of loss tangent, tan δ, related with lattice vibrations) of diamond containing single neutral vacancies in all possible spin states are calculated in the framework of the same space group symmetry using the first principles LCAO method and the hybrid B3LYP functional. The choice of system symmetry when modeling point defects by the CRYSTAL computer code using the periodic supercell (SC) approach has been considered in detail. The effect of the vacancy on the Raman and IR absorbance spectra is analyzed. Results of our calculations are compared with other calculations and existing experimental data. It is shown that vacancies do not affect tan δ at far IR region planned to be used in diamond windows in fusion reactors for plasma heating and stabilization.

1. Introduction

Diamond is widely used material, not only as gemstone and attractive for fundamental science but also for numerous innovative applications such as quantum technologies, sensors, radiation detectors, nanoscale chemical and biomedical imaging, as well as green and sustainable technologies [1–7]. As the result of the development of high-pressure high temperature (HPHT) diamond synthesis and chemical vapor deposition (CVD) techniques, synthetic diamond has gained significant scientific and economic importance. Both single crystals and polycrystalline diamonds could be grown on multiple surfaces with variable grain sizes. Polishing of these surfaces allows for the development of atomically flat diamond films, whereas reactive ion etching and CVD growth on patterned templates result in different diamond nanostructures such as nanowires, diamond foams, fibers, etc.

Moreover, the conductivity of diamond, which is an insulating material with the wide bandgap of 5.5 eV, can be tuned by substituting carbon atoms in the crystal lattice with boron or nitrogen and phosphorus to obtain p-type or n-type conductivity, respectively [8]. At rather low doping levels, diamond attains semiconducting properties, while higher doping levels result in a semi-metallic electrical behavior.

In combination with diamond unique intrinsic properties, i.e., an extreme hardness, high thermal conductivity, chemical inertness, broad potential window and biocompatibility, this has led to a broad range of applications. Boron-doped diamond, for example, could serve as an electrochemical material [9]. It holds a great potential for high power electronics [10] and photodetectors [11], and plays a major role in quantum technologies [12]. Over the past ten years, diamond has also been gaining more and more interest as a photocathode material for alternative p-type dye-sensitized solar cells (DSSCs) and for photocatalytic applications.

Diamond's optical applications are related to the *color centers*, such as the vacancies V^0, combined with impurities, e.g., NV^0 [13]. These centers can be used not only for sensing magnetic and electric fields but also for quantum information technology. Progress in this field relies on substantial advances in the production of highly controlled diamond materials with low defect density using CVD or HPHT techniques. In particular, diamond windows are used in fusion reactors for plasma heating and diagnostic. In this case, materials with low dielectric losses are in great demand. High quality CVD diamonds demonstrate very low loss tangent ($\sim 10^{-6}$ at 170 GHz) and meet these requirements [14–16]. However, the important question remains open, how defects, in particular, as-grown or radiation-induced vacancies could affect diamond dielectric properties (first of all, loss tangent).

* Corresponding author.
** Corresponding author. Institute of Solid State Physics, University of Latvia, 8 Kengaraga Str., LV-1063, Riga, Latvia.
E-mail addresses: leorus@inbox.lv (L.L. Rusevich), kotomin@latnet.lv, E.Kotomin@fkf.mpg.de (E.A. Kotomin).

Recently, several first principles calculations were performed for diamond with dopants and point defects [17–29], including neutral monovacancies [22–26], with the focus on the effects in the electronic structure. Note that despite its technological importance, only a few theoretical studies so far dealt with the first principles calculations of the vibrational properties of defects [18–22,27–31] and relevant loss tangent [21] in insulating materials. As far as we know, there are no calculations of both the IR spectra and the loss tangent for single vacancies in diamond.

In this paper, we present the results of theoretical study focused on the *dielectric properties* (epsilon and loss tangent) of vacancies in different spin states that is important, in particular, for the use in optical applications, as windows for microwave plasma heating in fusion reactors, and high power electronics.

2. Computational details

First-principles (*ab initio*) computer simulations of diamond crystal with a common irradiation-induced point defect — an isolated neutral carbon vacancy — have been performed within the linear combination of atomic orbitals (LCAO) approximation of the density functional theory (DFT), as implemented in CRYSTAL17 computer code [32,33]. The pristine diamond has *Fd-3m* space group symmetry (SG 227) with atoms in the 8a(1/8,1/8,1/8) Wickoff position. The commonly used crystallographic cubic cell of such crystal lattice contains 8 atoms, whereas the primitive unit cell consists of only 2 atoms. A periodic supercell (SC) approach has been applied to model a defective diamond. The simulations were performed for a cubic 2 × 2 × 2 SC, consisting of 8 crystallographic cells and containing 64 carbon atoms before vacancy creation. Defect was generated by removing one carbon atom from SC to create a vacancy, which concentration, in this case, is 1/64 ≈ 1.56% ($\approx 2.75 \bullet 10^{21}$ cm ^{3}) with a distance between the nearest defects is ~7.2 Å. The same SC was used previously for the simulation of an isolated nitrogen substitutional atom (*C-center*) in diamond [21].

In this study, the structural, electronic, vibrational (the transverse optical phonon frequencies) and dielectric properties of diamond with an isolated neutral vacancy in all possible spin states were investigated. The defect-induced one-phonon Raman and infrared (IR) spectra were simulated as well.

The computations were performed with three-parameter global hybrid exchange-correlation functional B3LYP, which combines BECKE exchange functional with 20% (by default) of exact Hartree-Fock (HF) exchange and LYP (Lee-Yang-Parr) correlation functional with NONLOCAL parameters 0.9 and 0.81 (by default) [33,34]. Carbon atoms were described with all-electron basis set of Gaussian type functions with exponent for d-shell [35]. This basis set contains (6s)-(2sp)-(1sp)-(1d) contractions and is available on the CRYSTAL Basis Sets Library web site [36] as C_6-21G*_dovesi_1990 basis set. We have shown recently [21] that this combination of functional and basis set exhibits the best agreement between the calculated lattice constant, band gap and Raman peak position for a pristine diamond with the available experimental data. The five threshold parameters control the accuracy of the calculation of the bielectronic Coulomb and HF exchange series (truncation criteria) [33] have been set to 8, 8, 8, 8, 16. A regular Monkhorst-Pack mesh of points in the reciprocal space has been used for calculations with shrinking factor 4. The integrations were performed on a default predefined “extra large” pruned grid (XLGRID) consisting of 75 radial points and a maximum of 974 angular points in the regions relevant for chemical bonding. The Self-Consistent Field (SCF) convergence threshold parameter for the total energy was set to 10 ^{10} Hartree in all calculations.

The formation of a vacancy in the tetrahedrally coordinated diamond generates four dangling bonds (and four unpaired spins) at four, nearest to the vacancy, carbon atoms. In the open-shell simulations of systems with unpaired spins, all electrons are divided into two groups: with spins up (α-electrons) and spins down (β-electrons). The total spin of a system depends on the difference in the numbers of α- and β-electrons. As the result, three different spin states of the system may be realized after a vacancy creation: spin projections $S_z = 0$ (two α- and two β-electrons), $S_z = 1$ (three α- and one β-electrons) or $S_z = 2$ (four α-electrons). In the present paper, all possible spin configurations of an isolated neutral vacancy in diamond have been considered in the framework of the unrestricted (open shell) DFT calculations [33].

A complete *vibrational analysis* was performed here for three spin states of diamond with a vacancy. The transverse optical (TO) vibrational frequencies and vibrational contribution to the dielectric tensor were calculated within the harmonic approximation in the center of the first Brillouin zone (at the Γ-point). The complex dielectric function is the sum of the electronic (high-frequency) and vibrational components $\varepsilon(\nu) = \varepsilon_{el} + \varepsilon_{vib}(\nu)$ and it is calculated in CRYSTAL code on the basis of a classical dispersion relation of Drude-Lorentz model [33]. The electronic part is calculated through the Coupled Perturbed Hartree-Fock/Kohn-Sham (CPHF/CPKS) scheme, adapted for periodic systems [37,38]. The integrated intensity of each IR-active vibrational mode was computed under the hypothesis of isotropic response. For the comparison, intensities of IR-active modes were calculated by means of two methods — the Berry phase approach, which implies numerical differentiations, and the CPHF approach, which is fully analytical [33,39]. Both methods demonstrate close results, discrepancies do not exceed ~5%. The relative intensities of the Raman-active modes were computed by a fully analytical method [40,41]. Additionally, the defect-induced one-phonon Raman and IR absorbance spectra were simulated using corresponding TO vibrational modes. Both types of spectra were calculated as a convolution of intensities with the Lorentzian resolution function (FWHM = 8 cm ^{1}). Besides that, the dielectric functions and loss tangent of diamond with vacancies associated with the vibrational modes were calculated.

3. Results and discussion

3.1. Choice of supercell symmetry for a system with a point defect

In simulations with using of CRYSTAL computer code an important computational issue is a choice of the symmetry for the crystal with a defect. First of all, a full geometry optimization of SC is performed during an investigation. The results of this optimization depend on the symmetry, therefore, its choice may affect some important parameters of the system (structural, electronic and vibrational properties, total energy, spins localization, vacancy formation energy etc.). Generally, the symmetry of a system is reduced upon the creation of a defect. Moreover, the final symmetry of the system may additionally decrease due to the presence of atoms with different spins. Note that in CRYSTAL code both the number of atoms in the SC and the exact position of the point defect within the SC define the symmetry of the defective system. In fact, all atoms in SC are divided into several sets of symmetry equivalent atoms and, additionally, there may be a few atoms in SC, which have no equivalent by symmetry atoms [42,43]. In our case, 64 atoms of SC are distributed into the following sets of symmetry equivalent atoms: 4 sets of 12 atoms, 2 sets of 4 atoms, 2 sets of 3 atoms, and another 2 atoms have no symmetry equivalent atoms.

Fully relaxed 64-atom SC, corresponding to the pristine diamond and used in our simulations, is presented in Fig. 1. To demonstrate that symmetry of the resulting defective system depends on the choice of the atom for vacancy creation, let us discuss, for example, two highlighted in this figure carbon atoms — C33 and C34. Atom C33 has no equivalent by symmetry atoms and its removal from the SC does not change the symmetry of the system. To take into account spin states of defective system, it is necessary to consider the nearest to the vacancy atoms — C1, C4, C13 and C27 — which have unpaired spins after removal of a C33 atom. These four atoms are equivalent by symmetry both in pristine SC and in SC without C33. Therefore, for the system with $S_z = 2$, when all four mentioned atoms have the same spin and remain equivalent, the

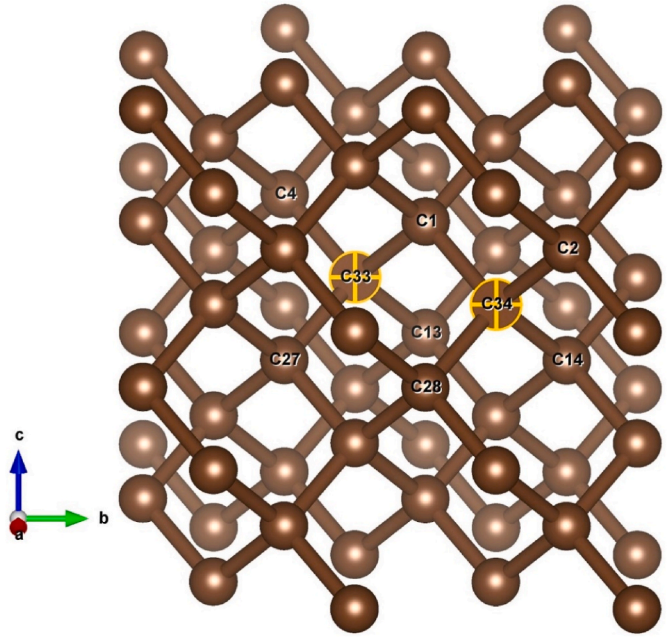

Fig. 1. Fully optimized 64-atom supercell, corresponding to the pristine diamond, used for simulations of a vacancy in diamond.

symmetry remains the same as in a pristine system. However, for cases $S_z = 1$ and $S_z = 0$, the symmetry is reduced due to the presence of atoms with different spins. Indeed, SC with $S_z = 1$ has 6 symmetry operations (instead of 24 for pristine SC) and corresponds to the trigonal crystal system (SG 160), whereas SC with $S_z = 0$ has only 4 symmetry operations (SG 35, orthorhombic crystal system). Thus, defective system with a vacancy in the position of C33 atom has the highest possible symmetry for a given SC, which allows us to reduce the computational cost of simulations, but demands to consider different spin states at different symmetries. In other words, artificial constraints, imposed by symmetry, are different for different spin states. In our previous study [21], where we considered defective diamond with the *C-center*, a nitrogen atom replaced namely C33 atom in the SC. However, in this case, the defect had only one spin state.

In contrast to C33, atom C34 has 11 (it is maximum for a given 64-atom SC) equivalent by symmetry atoms. After vacancy creation in the position of this atom, the nearest to the vacancy atoms C14 and C28 (Fig. 1) are equivalent by symmetry, while atoms C1 and C2 have no equivalent partners. In this case, the SC has only 2 symmetry operations and corresponds to the monoclinic crystal system (SG 8). While considering spin state $S_z = 2$, the symmetry of a system remains the same (SG 8), but for spin states $S_z = 1$ and $S_z = 0$ the symmetry either does not change (SG 8; C14 and C28 atoms have the same spins) or reduced down to SG 1 (C14 and C28 atoms have different spins). Thus, vacancy formation in the position of C34 atom allows us to consider all three spin states in the framework of the symmetry of the same space group. In this study, we simulated a vacancy in the position of C34 atom and considered all spin states of a defective diamond within the SG 8 symmetry. Thus, the symmetry constraints are the same for all spin states, which allows us correct comparison of the simulation results for different states. At the same time, we do not resort to calculations without symmetry (SG1), which would greatly increase the computational cost, taking into account that calculations with spins are already extremely demanding on computer resources.

3.2. Total energies, vacancy formation energies, structural and electronic properties

In this study, diamond crystal with neutral vacancies in all possible spin states have been simulated. The calculations performed for the spin $S_z = 2$ by using the hybrid B3LYP functional with standard 20% of exact HF exchange exhibit a metallic solution (conducting state). However, a minimal increase of exact HF exchange percentage till 24% is sufficient for getting the insulating state (similarly to the case [23]). Therefore, for spin states $S_z = 0$ and $S_z = 1$ we performed calculations with 20% of HF exchange, whereas the insulating state of diamond with the vacancy in spin state $S_z = 2$ was simulated by B3LYP functional with 24% of HF exchange. To check the dependence of the results on the percentage of HF exchange, calculations were performed for both 20% and 24% of HF exchange. Note that standard percentage of HF (20%) gives better agreement between calculated and experimental parameters of a pristine diamond (see Table 1).

Computations reveal that diamagnetic singlet state $S_z = 0$ has the minimal total energy, in agreement with experiments [23,45]. The triplet state $S_z = 1$ has a slightly higher energy (the difference $\Delta E_{01} =$ 0.12 eV), while much large difference occurs between the quintet state ($S_z = 2$) and the ground state ($S_z = 0$) — $\Delta E_{02} = 1.44$ eV (20% of HF exchange, conducting state for $S_z = 2$). These conclusions coincide with the results of the previous calculations by means of the PBE0, B3LYP and HSE06 functionals (CRYSTAL computer code) in Ref. [23] ($\Delta E_{01} = 0.13$ eV, $\Delta E_{02} = 1.39 \div 1.40$ eV) and by the HSE06 functional (VASP computer code) in Ref. [25] ($\Delta E_{01} = 0.14$ eV, $\Delta E_{02} = 1.46$ eV). Note that in the simulations of all spin states with the B3LYP functional with 24% of HF exchange, the stability sequence of states does not change and the differences between the ground state ($S_z = 0$) and the states $S_z = 1$ and $S_z = 2$ (insulating state) remain almost the same: $\Delta E_{01} = 0.12$ eV and $\Delta E_{02} = 1.40$ eV.

The formation energy of the isolated neutral vacancy E_{vac} was calculated as

$$E_{vac} = E(\text{defective}) + E(\text{C}) - E(\text{pristine}), \quad (1)$$

where E(defective) and E(pristine) are the total energies of the defective (with a vacancy) and pristine diamond supercells, E(C) is the energy of a single carbon atom in the pristine diamond [23–25]. As the result, the vacancy formation energies are as follows: 6.78 eV ($S_z = 0$), 6.90 eV ($S_z = 1$) and 8.22 eV ($S_z = 2$, conducting state, 20% of HF exchange). At the same time, the vacancy formation energies increase minimally for 24% of HF exchange: 6.86 eV ($S_z = 0$), 6.98 eV ($S_z = 1$) and 8.26 eV ($S_z = 2$, insulating state). The presented results are in a very good agreement with the data from Table 3 (for the hybrid functionals) and Table 4 in Ref. [23] and from Table 1 (for the HSE06 functional) in Ref. [25].

Vacancy creation disturbs crystal lattice and changes the electronic properties of a system. We suppose that the nearest to the vacancy atoms — C1, C2, C14 and C28 — have unpaired spins. The initial guess for the distribution of these spins was as follows (Fig. 2, red arrows): for $S_z =$ 0 (Fig. 2a) spins at C1 and C2 atoms are $\mu_s =$ 1 electron spin (unpaired β-electron at each atom), but at C14 and C28 atoms $\mu_s = +1$ (unpaired α-electron at each atom); for $S_z = 1$ (Fig. 2b) C1 atom has spin $\mu_s =$ 1 while C2, C14, C28 atoms have spin $\mu_s = +1$ each; for $S_z = 2$ (Fig. 2c) all four atoms have spin $\mu_s = +1$.

During full geometry optimization, the resulting charge and spin distributions could change. These results and SC volume, depending on the spin state and percentage of HF exchange in the functional, are presented in Table 2. All data therein, as well as calculations of total and formation energies, show that computations with 20% and 24% of HF

Table 1
Lattice constant a, band gap E_g and position of a Raman peak for a pristine diamond, calculated with using of 20% and 24% of HF exchange in the B3LYP functional. "Expt." — experimental values [2,7,44].

	20% of HF exchange	24% of HF exchange	Expt.
a, Å	3.589	3.584	3.567
E_g, eV	5.7	6.0	5.5
Raman peak, cm ^{1}	1332	1345	1332

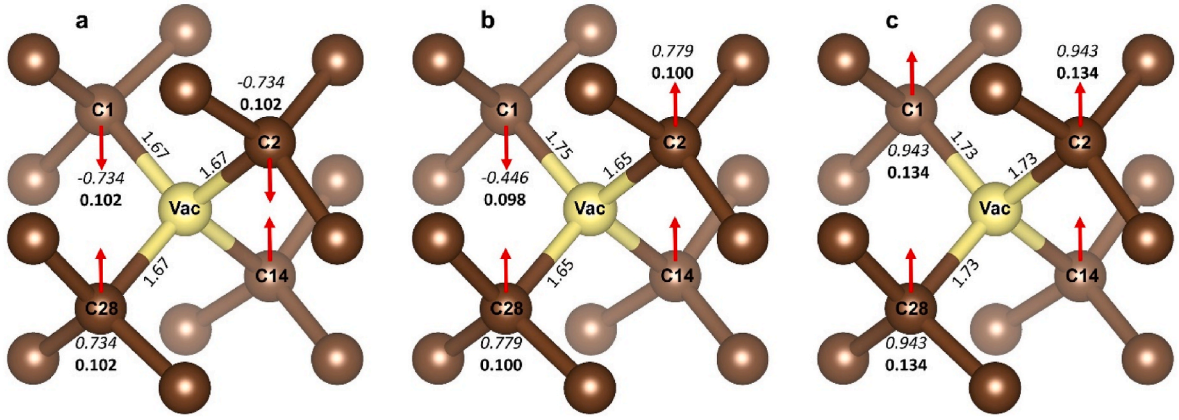

Fig. 2. The nearest vicinity of the vacancy (in the position of C34 atom; yellow ball) in the relaxed defective diamond SC. The resulting bond length (in Å), atomic spin (in |e|, *italic*; red arrows — direction) and Mulliken charge (in |e|, **bold**) are presented for the symmetry nonequivalent atoms, adjacent to the vacancy. (**a**) Spin state S_z 0; (**b**) S_z 1; (**c**) S_z 2. Carbon atoms C14 and C28 are equivalent by symmetry; thus, only direction of spin is shown for C14 atom.

Table 2
Calculated SC volume V for the pristine and defective systems, spin μ_s and Mulliken charge q for the nearest to the vacancy atoms depending on system spin state and percentage of HF exchange in the functional.

	20% of HF exchange	24% of HF exchange
V of pristine SC, Å^3	369.76	368.44
	$S_z = 0$	
V, Å^3	370.47 (+0.19%)	369.19 (+0.20%)
μ_s, |e| (for C1, C2)	0.734	0.759
μ_s, |e| (for C14, C28)	0.734	0.759
q, |e| (for C1, C2, C14, C28)	+0.102	+0.104
	$S_z = 1$	
V, Å^3	370.42 (+0.18%)	369.15 (+0.19%)
μ_s, |e| (for C1)	0.446	0.490
μ_s, |e| (for C2, C14, C28)	0.779	0.800
q, |e| (for C1)	+0.098	+0.099
q, |e| (for C2, C14, C28)	+0.100	+0.103
	$S_z = 2$	
V, Å^3	372.43 (+0.72%)	371.11 (+0.72%)
μ_s, |e| (for C1, C2, C14, C28)	0.933	0.943
q, |e| (for C1, C2, C14, C28)	+0.132	+0.134

give close results. Therefore, hereafter, unless another is said, spin states $S_z = 0$ and $S_z = 1$ are studied with 20% of HF, whereas spin state $S_z = 2$ — only with 24% of HF exchange (non-conducting state). Let us emphasize once again that state $S_z = 2$ is a high-excited state (see above) and is rather of theoretical interest. As far as we know, this state is not observed experimentally.

The calculations (Table 2) reveal well localized electron spins on four atoms adjacent to the vacancy for spin states $S_z = 0$ (Fig. 2a) and, especially, $S_z = 2$ (Fig. 2c). Moreover, the spins of these atoms are either the same ($\mu_s = 0.943$ for $S_z = 2$) or equal in the absolute value ($\mu_s = \pm 0.734$ for $S_z = 0$). Different situation occurs for the spin state $S_z = 1$ (Fig. 2b). While for three atoms with unpaired α-electrons spins are equal and well localized ($\mu_s = 0.779$), spin of atom C1 with β-electron is only $\mu_s =$ 0.446. The missing half of the electron spin is redistributed in SC among many atoms, which, in general, are not close to the vacancy. Note that these conclusions on spin distributions are confirmed by the calculations with both 20% and 24% of HF exchange. Note also that similar peculiarities of spin localization were reported for computations with the B3LYP functional in Ref. [23].

Let us consider now the changes of atomic charges due to formation of a neutral vacancy. As Table 2 and Fig. 2 show, four nearest to the vacancy atoms get a positive charge in all three spin states (moreover, these atoms are the most positively charged). The Mulliken population analysis reveals that charges of these atoms are ~ +0.1|e| for the $S_z =$ 0 and $S_z = 1$ states and +0.134|e| for the state $S_z = 2$. At the same time, charges of all carbon atoms in the second shell around a vacancy are slightly negative for all spin states. Namely, they equal 0.042|e| for the state $S_z = 2$; 0.024|e| for three atoms which are near C1 atom (with β-electron) and 0.031|e| or 0.035|e| for atoms which are near atoms with α-electrons in system with $S_z = 1$; 0.030|e| or 0.031|e| for atoms of the second shell for the spin $S_z = 0$. As the result, a total charge of atoms within two shells around a vacancy is +0.040|e| for $S_z = 0$, +0.035|e| for $S_z = 1$ and + 0.032|e| for $S_z = 2$. These values are 1.5–2 times larger those for the defective diamond with the *C-center* [19,21]. However, even in the vacancy case, the charges of the third shell atoms have both positive and negative signs and do not exceed 0.017|e| in absolute value for all three spin states, and defective systems demonstrate almost complete charge neutrality already inside these three shells around the defect.

It is interesting to consider from this point of view the *structural distortions* of the lattice caused by a vacancy. Our simulation reveals that in pristine diamond C–C distance is 1.554 Å (1.552 Å for 24% of HF exchange) with the volume of the perfect 64-atom SC 369.76 Å^3 (368.44 Å^3 for 24% of HF). After a vacancy creation, the nearest carbon atoms move away from the vacancy in all spin states. The calculations give the following distances from the vacancy to four adjacent atoms (Fig. 2): ~1.67 Å (+7% relative to the bond length in the pristine diamond) for $S_z = 0$; 1.75 Å (+13%) for C1 atom (with β-electron) and 1.65 Å (+6%) for three atoms with α-electrons at $S_z = 1$; ~1.73 Å (+11%) for spin state $S_z = 2$. In its turn, the distances between atoms of the first and second shells are shorter than in the pristine diamond. These distances fall within 1.50–1.52 Å (3% to 2%) for $S_z = 0$ and $S_z = 1$ and 1.50 Å (3%) for $S_z = 2$. Simultaneously, the bond lengths between atoms of the second and third shells are practically restored to those in a defect-free lattice: 1.55–1.57 Å ($S_z = 0$ and $S_z = 1$) and 1.56 Å ($S_z = 2$). Thus, the dependence of structural changes on the spin states is strongly expressed only for the first shell around a vacancy (the nearest four atoms), the local perturbations of the lattice decay rapidly and after the third shell the lattice distortion, caused by a vacancy, almost completely disappears.

Note also, that in general, a vacancy increases the volume of unit cell in all spin states. Our simulations of 63-atom defective SC give the following SC volumes: 370.47 Å^3 (+0.19%, $S_z = 0$), 370.42 Å^3 (+0.18%, $S_z = 1$) and 371.11 Å^3 (+0.72%, $S_z = 2$). The largest increase of SC volume for the system with spin state $S_z = 2$ can be explained by the Pauli exclusion principle, considering the presence of very well localized electrons with identical spins at the atoms closest to the vacancy.

At the end of this subsection, let us discuss the electronic density of state (DOS) for the different spin states of a defective diamond. Calculated DOS for spins $S_z = 0$, $S_z = 1$ and $S_z = 2$ are presented in Figs. 3–5, respectively.

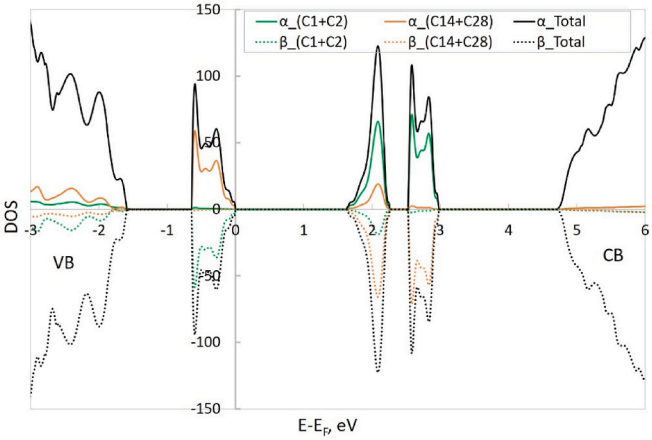

Fig. 3. Projected and total electronic DOSs of α- and β-electrons for diamond with a neutral vacancy. Spin state S_z 0. The zero energy value corresponds to the Fermi level. Contributions to total DOSs of four nearest to the vacancy carbon atoms are presented. Part of valence band (VB), in-gap defect bands and part of conducting band (CB) are shown.

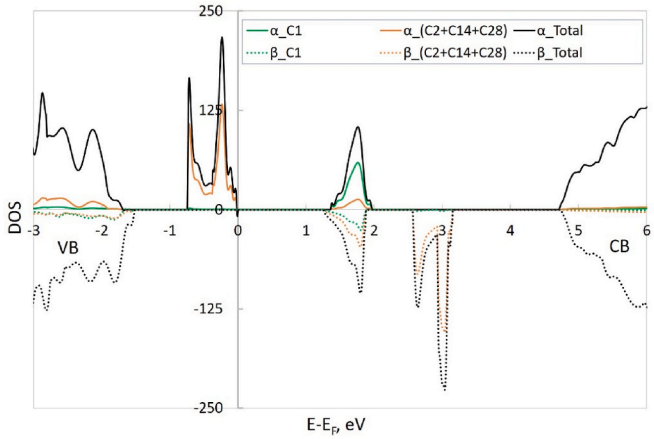

Fig. 4. Projected and total electronic DOSs of α- and β-electrons for diamond with a neutral vacancy. Spin state S_z 1. The zero energy value corresponds to the Fermi level. Contributions to total DOSs of four nearest to the vacancy carbon atoms are presented. Part of valence band (VB), in-gap defect bands and part of conducting band (CB) are shown.

The calculated indirect band gap of a perfect diamond equals 5.7 eV (6.0 eV for 24% of HF exchange) which is close to the experimentally observed value of 5.5 eV. However, defect modifies the band gap. As one can see in Figs. 3–5, a neutral vacancy produces inside the band gap the occupied energy states (bands) above the valence band (VB) top and unoccupied defect bands in the middle of the band gap, closer to the conduction band (CB). The simulations reveal that all in-gap defect bands are mainly produced by the adjacent to the vacancy carbon atoms (where unpaired spins are mainly localized). Additionally, the band gap (the energy difference between the VB top and the CB bottom) of a defective system in all spin states is slightly increased compared to defect-free diamond.

Now let us consider in more detail the electronic DOS of diamond with a neutral vacancy in different spin states. In spin state $S_z = 0$, total DOSs corresponding to α- and β-electrons essentially coincide (Fig. 3). In this state, C14 and C28 carbon atoms carry well localized unpaired α-electrons, whereas unpaired β-electrons have the same degree of localization on C1 and C2 atoms (see Table 2). Therefore, the occupied defect band of α-electrons are mainly produced by C14 and C28 atoms, but occupied defect band of β-electrons — by C1 and C2 atoms. These

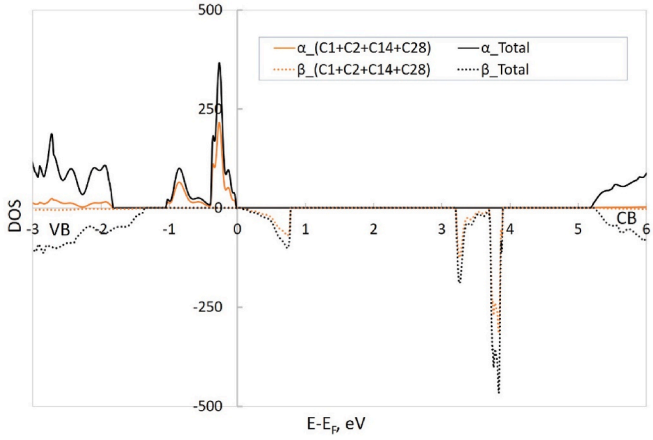

Fig. 5. Projected and total electronic DOSs of α- and β-electrons for diamond with a neutral vacancy. Spin state S_z 2. The zero energy value corresponds to the Fermi level. Contributions to total DOSs of four nearest to the vacancy carbon atoms are presented. Part of valence band (VB), in-gap defect bands and part of conducting band (CB) are shown.

defect bands are located ≈0.9 eV above the VB top, and their dispersion (width of the band) is ≈ 0.6 eV. At the same time, states of missing β-electrons on C14 and C28 atoms and α-electrons on C1 and C2 atoms mainly form in-gap unoccupied defect bands clearly observed in Fig. 3. The energy difference between the top of occupied defect band and bottom of nearest unoccupied defect band is ≈ 1.6 eV and transition between these two bands are indirect both for α- and β-electrons. Wherein, the band gap for spin $S_z = 0$ is ≈6.3 eV. Note, that the interaction of the periodically repeated defects is characterized by dispersion of the defect band. In our case (SC 2 × 2 × 2) this dispersion has quite acceptable value (~0.6 eV), taking into account the total band gap width (~6 eV).

The spin state $S_z = 1$ is interesting in the sense that there is only one occupied defect band, corresponding to α-electrons, inside the band gap (Fig. 4). This band is mainly produced by the α-electrons of C2, C14 and C28 atoms and lies ≈1 eV above the VB top. C1 atom with a low degree of spin localization of β-electron ($\mu_s =$ 0.446), does not form occupied defect level inside the band gap (it gives contribution to the VB). Although, the missing fraction of spin of β-electron on C1 atom takes part in formation of unoccupied defect band of β-electrons in the middle of the band gap. At the same time, states of missing α-electron on C1 atom, as well as the states of missing β-electrons on C2, C14 and C28 atoms, produce unoccupied defect bands inside the band gap. The gap between occupied and unoccupied bands for α-electrons is ≈ 1.4 eV, it is indirect transition. The width of indirect transition between VB and the first unoccupied defect band of β-electrons is ≈ 2.8 eV, while band gap of defective diamond in this spin state is ≈ 6.3 eV (approximately the same as for $S_z = 0$).

Lastly, the vacancy with spin $S_z = 2$ has only one in-gap occupied defect gap (for α-electrons), which is mainly produced by C1, C2, C14 and C28 atoms, and is located ≈ 0.8 eV above the VB top for α-electrons (Fig. 5). The energy gap between this band and CB is ≈ 5.2 eV (the indirect transition). The states of missing β-electrons form two in-gap unoccupied defect bands. The energy gap between the top of VB for β-electrons and the bottom of the nearest unoccupied defect band is ≈ 1.4 eV and the transition between them is indirect. In this spin state, band gaps for α- and β-electrons are slightly different: ≈7 eV for α-electrons and ≈6.6 eV for β-electrons (compare with 6 eV for the pristine diamond band gap calculated with 24% of HF exchange).

In general, it can be concluded that the calculated dispersions of the defect bands and their positions within the diamond band gap for all spin states (Figs. 3–5) are in good agreement with previous first principles calculations [23,25].

3.3. Vibrational properties, IR and Raman spectra

A complete vibrational analysis was performed for the defective diamond with a vacancy in three spin states. The TO vibrational frequencies and relevant the IR and Raman intensities were calculated, as well as the one-phonon Raman and IR spectra were simulated. There are 189 normal lattice vibrations at the Γ-point of 63-atom SC of the defective diamond. Three of them are acoustic vibrations, the others — optical. Because calculations are performed at low symmetry (SG 8), all vibrational modes are nondegenerate, i.e., there are 186 TO modes in the system with a vacancy. Moreover, all these modes are IR- and Raman-active. However, most of them have very small, close to zero, intensities and their contributions to the corresponding spectra are negligible. Calculated TO modes, depending on the spin states of defective system, fall into the following frequency ranges: 435–1348 cm ^{1} ($S_z = 0$), 445–1343 cm ^{1} ($S_z = 1$) and 492–1348 cm ^{1} ($S_z = 2$).

Defect-free diamond reveals no IR activity (forbidden by symmetry), but it appears due to defects. The calculated IR spectra (the one-phonon area) caused by a vacancy with spins $S_z = 0$ and $S_z = 1$ are presented in Fig. 6. As can be seen, these spectra have many peaks at different frequencies, more or less uniformly distributed over the wide energy spectrum. If in $S_z = 0$ case it is possible to speak about a few dominant peaks (1042 cm ^{1}, 1113 cm ^{1} and 1316 cm ^{1}), in the $S_z = 1$ case the intensities of most peaks do not differ so much. Spectrum for spin $S_z = 2$ is not shown here because it is qualitatively similar to those in Fig. 6, but peak intensities are several times smaller, even relative to the spectrum at $S_z = 0$. Generally, spin state $S_z = 2$ of a defective system is "the closest" to pristine diamond because of its maximum "symmetry" of spins. Therefore, intensity of IR spectrum for $S_z = 2$ is minimal (in a pristine diamond this intensity is zero). We face this effect again below, when discuss Raman spectra and dielectric properties of the defective systems in different spin states.

An analysis of the atom displacements in the normal modes that form the spectral peaks as well as the isotopic substitution method (the possibility to change the atomic masses of specific atoms as implemented in the CRYSTAL code [33]) reveal that the vibrations of four atoms adjacent to the vacancy do not play a significant role in the formation of mentioned above main IR peaks. In particular, we have calculated for different spin states the isotopic shifts of vibrational modes due to $^{12}C \rightarrow {}^{13}C$ substitution for atoms C1, C2, C14 and C28. In general, the conclusion can be drawn that IR spectra arise due to the common perturbation of the crystal lattice caused by a vacancy, whereas the nearest neighbors of the vacancy do not make the crucial contribution to the spectra. This conclusion confirms the results of the study [22]. Interestingly, that situation with the *C-center* is opposite. The vibrations of N atom and the closest to it carbon atoms substantially contribute to the IR spectrum [21].

The vibrations of four atoms adjacent to the vacancy give the largest contribution to the IR spectra in the low-frequency spectral region (below about 750 cm ^{1}). The region 750–1050 cm ^{1} may be characterized by a small contribution of the nearest to the vacancy carbon atoms, while in the frequency range above 1050 cm ^{1} the effect of mentioned atoms is again increased. This conclusion is valid for both spin states. Among all peaks of noticeable intensity in the spectra shown in Fig. 6, the first two peaks in each spectrum (435 cm ^{1} and 494 cm ^{1} for $S_z = 0$, 446 cm ^{1} and 463 cm ^{1} for $S_z = 1$) have maximal contribution from the nearest neighbors of the vacancy. These peaks are formed by the vibrational modes with isotopic shifts about 7 cm ^{1}. In reality, some modes have isotopic shift even more than 10 cm ^{1}, but, at the same time, the intensities of corresponding IR peaks are close to zero.

The Raman spectrum of a pristine diamond demonstrates a single sharp peak at 1332 cm ^{1}, which is associated with a triply degenerate TO phonon mode of F_{2g} symmetry. Our simulations perfectly agree (at least, at 20% of HF exchange) with the experimental data (see Table 1). The simulated Raman spectra (the one-phonon area) of diamond with the vacancy in spin states $S_z = 0$ and $S_z = 1$ are presented in Fig. 7. These spectra look like "perturbed" spectrum of a pristine diamond: a single dominant peak (shifted to the red side relative to the peak position in a perfect crystal) and large number of peaks with significantly lower intensities in the range of existing vibrational modes. We again do not provide here a spectrum for the spin state $S_z = 2$ because it is even "closer" to the spectrum of a pristine diamond: number of small peaks is less and their intensities relative to a dominant peak are lower. Thus, we are again faced with the situation that spin state $S_z = 2$ of the defective diamond is "the closest" to the pristine diamond. However, the red shift effect is inherent to this state to the fullest (see below).

Main peaks of the Raman spectra in Fig. 7 (1316 cm ^{1} for $S_z = 0$ and 1318 cm ^{1} for $S_z = 1$) are formed mostly by vibrational modes with isotopic shifts about 3 cm ^{1}. Note, that the last peaks with significant intensities of IR spectra in Fig. 6 are formed by the same modes.

The main spectral feature of the Raman spectra of diamond with a vacancy is a redshifting of the first-order peak compared to the perfect diamond. Dependence of the first-order Raman peak position on the defect concentration was studied both experimentally [46,47] and theoretically [22] (for spin state $S_z = 0$ only). All investigations reveal the linear dependence of the peak shift on the defect concentration. However, slopes of lines, obtained in the experimental works, as well as

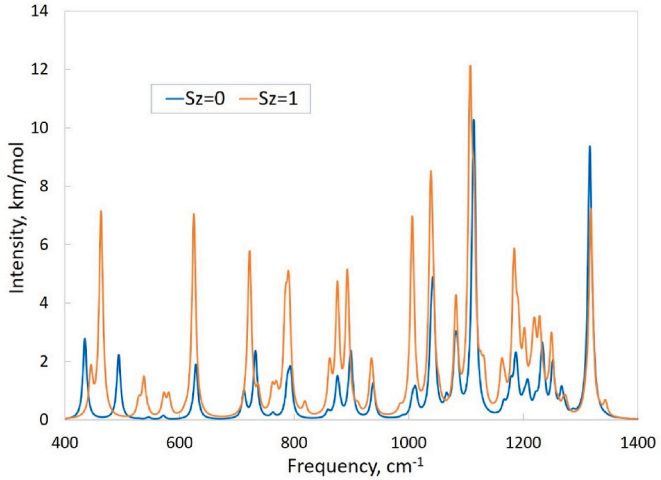

Fig. 6. The simulated one-phonon IR absorbance spectra of diamond with a neutral vacancy for spin states S_z 0 and S_z 1.

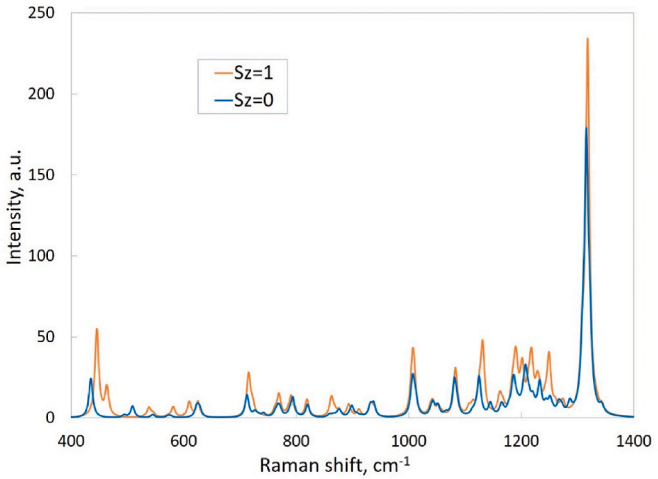

Fig. 7. The simulated Raman spectra of diamond with a neutral vacancy for spins S_z 0 and S_z 1.

considered concentrations, vary quite a lot [22]. Our simulations give the following red shift of the first-order Raman peak depending on the spin states: 16 cm ^{1} (1332 cm ^{1} → 1316 cm ^{1}) for $S_z = 0$, 14 cm ^{1} (1332 cm ^{1} → 1318 cm ^{1}) for $S_z = 1$ and 14 cm ^{1} (1345 cm ^{1} → 1331 cm ^{1}, 24% of HF exchange) for $S_z = 2$. These values very well coincide with red shift, calculated in Ref. [22] for $S_z = 0$ and vacancy concentration $\approx 2.75 \bullet 10^{21}$ cm ^{3}, and they are between the experimental values, obtained for similar concentrations. In conclusion, we emphasize that the red shift of the peak almost does not depend on the spin state. Note that the vacancy concentration in our simulations (1.56%) is corresponding to experiments [46–48], at least in the case of vacancy formation due to irradiation that is of interest for us.

3.4. Dielectric properties

Our calculations give $\varepsilon = 5.5$ for the relative permittivity of a pristine diamond. In this case, the permittivity is a constant, which is fully determined by the electronic component (the optical dielectric constant ε_{el}): no vibrational contribution, no dependence on the frequency of the electric field, no absorption, no IR spectrum. This result is obtained for the calculations with both 20% and 24% of HF exchange and very well agrees with the experimental data (e.g., $\varepsilon = 5.7$ [44]). However, the situation changes for a defective diamond. In this case, permittivity is a complex function with imaginary part, associated with the conductivity, which determines the absorption. Now the real and imaginary parts of permittivity $\varepsilon(\nu)$ depend on the field frequency, and the vibrational (lattice) contribution ε_{vib} to the relative permittivity and the IR spectrum arises. Actually, the relative permittivity is a second rank tensor for the defective diamond, but non-diagonal elements of the static dielectric tensor are very small. Calculated electronic contributions to the dielectric tensors of diamond with a vacancy are as follows: $\varepsilon_{el} = 6.2$ for spin states $S_z = 0$ and $S_z = 1$ and $\varepsilon_{el} = 5.6$ for $S_z = 2$ (cf. $\varepsilon_{el} = 5.5$ for pristine diamond). At the same time, a vibration contribution to the static relative permittivity exists but is small: $\varepsilon_{vib}(0)$ does not exceed 0.1 for $S_z = 0$ and $S_z = 1$ and $\varepsilon_{vib}(0) \approx 0.01$ for $S_z = 2$ (cf. $\varepsilon_{vib} = 0$ for pristine diamond).

Real Re[$\varepsilon(\nu)$] and imaginary Im[$\varepsilon(\nu)$] parts of the complex, frequency-dependent relative permittivity for the defective system with spin states $S_z = 1$ and $S_z = 2$ are presented in Fig. 8 (the maxima of the imaginary part of function correspond to frequencies of TO modes). It is clearly seen that Im[$\varepsilon(\nu)$] for $S_z = 2$ is approximately 5 times smaller compared to $S_z = 1$ and amplitude of changes of this function for $S_z = 2$ is significantly lower (the function is closer to a constant) than that for $S_z = 1$. Note, that dielectric functions for $S_z = 0$ (not presented here) are quite similar to $S_z = 1$.

The loss tangent (tan δ) was calculated to characterize possible dielectric losses in diamond with vacancies. The loss tangent is the ratio of the imaginary and real parts of the complex permittivity $\varepsilon(\nu)$: tan δ = Im[$\varepsilon(\nu)$]/Re[$\varepsilon(\nu)$] [49]. Fig. 9 exhibits the dependences of the loss tangent functions on the frequency for the defective system with spins $S_z = 1$ and $S_z = 2$. As one can see, tan δ for $S_z = 2$ is about factor of 5 less than for $S_z = 1$, what means smaller dielectric losses for spin state $S_z = 2$. Note, that loss tangent for a pristine diamond equals to zero. Thus, all results presented in this subsection, allow us to conclude again that the spin state $S_z = 2$ of defective diamond is "the closest" to the pristine diamond.

The general conclusion could be drawn that the main effect of a vacancy on the diamond dielectric properties is concentrated in the range 400–1400 cm ^{1} (region of the existence of vibrational modes), while beyond this frequency region the defect practically does not produce dielectric losses. Interestingly, peak values of tan δ for the system with a vacancy ($S_z = 1$) exceed almost twice that for diamond with the *C-center* [21].

4. Conclusions

This study provides a comprehensive description of the structural, electronic, vibrational (including simulations of one-phonon Raman and IR spectra) and dielectric (including loss tangent calculation) properties of diamond with an isolated neutral vacancy. The calculations were performed for all possible spin states in the framework of the same space group symmetry, which allows us for the correct comparison of the results for different spin states. We have predicted that singlet state $S_z = 0$ has the lowest total energy, triplet state $S_z = 1$ has only slightly higher energy (the difference is 0.12 eV), while the energy of quintet state ($S_z = 2$) is approximately 1.4 eV higher of the ground state ($S_z = 0$) energy. In all spin states the vacancy slightly increases the volume of unit cell and the distances between the vacancy and four adjacent atoms. The spins of unpaired electrons are rather well localized on the nearest to the vacancy atoms for all spin states, except for the atom with the unpaired β-electron in the case of $S_z = 1$. The band gap of a defective system in all spin states is slightly widened in comparison with defect-free diamond. At the same time, a neutral vacancy creates occupied and unoccupied in-gap defect bands, which are mainly produced by the nearest to the vacancy carbon atoms. However, the nearest neighbors of a vacancy do not make the crucial contribution to the IR absorbance spectra; these spectra arise rather due to the perturbation of the entire crystal lattice caused by a vacancy. The red shift of the first-order Raman peak does not depend on the system spin state. In general, most of diamond properties weakly depend on the vacancy spin state. On the other hand, in many aspects the spin state $S_z = 2$ of the defective diamond is "the closest" to the pristine diamond.

The defect-induced features in IR and Raman spectra as well as in dielectric functions arise in the same phonon range 400–1400 cm ^{1}, i.e., in the region of the existence of vibrational modes. An isolated neutral vacancy practically does not induce the dielectric losses outside this frequency range, what is important for diamond applications in fields of plasma monitoring and electron cyclotron resonance (ECR) heating in fusion reactors, for which essential range is 140–206 GHz (less than 7 cm ^{1}). Calculated loss tangent for this range is about 10 ^{6} for the spin

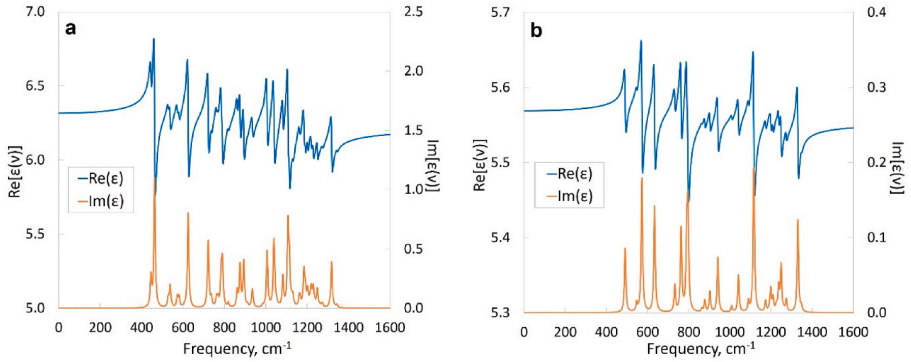

Fig. 8. Real Re[$\varepsilon(\nu)$] (left ordinate) and imaginary Im[$\varepsilon(\nu)$] (right ordinate) parts of relative permittivity for diamond with a vacancy. (**a**) Spin state S_z 1; (**b**) S_z 2.

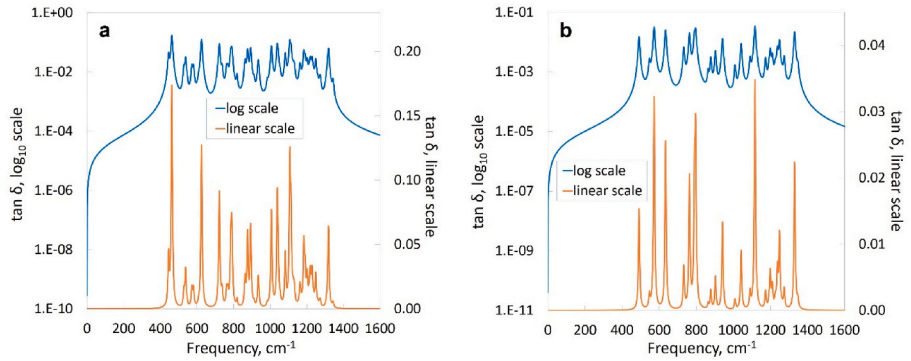

Fig. 9. Loss tangent (tan δ) for diamond with a vacancy in logarithmic (base 10, left ordinate) and linear (right ordinate) scales. (**a**) Spin state S_z 1; (**b**) S_z 2.

states $S_z = 0$ and $S_z = 1$. Thus, as grown or radiation induced vacancies do not affect above mentioned fusion reactor applications. However, "low" frequencies, perhaps, may be affected by the presence in diamond of vacancy clusters [50], which needs additional study.

CRediT authorship contribution statement

L.L. Rusevich: Writing – review & editing, Writing – original draft, Methodology, Investigation, Formal analysis. **E.A. Kotomin:** Writing – review & editing, Writing – original draft, Conceptualization. **A.I. Popov:** Project administration. **G. Aiello:** Investigation. **T.A. Scherer:** Supervision. **A. Lushchik:** Writing – review & editing, Supervision, Funding acquisition.

Declaration of competing interest

The authors declare that they have no known competing financial interests or personal relationships that could have appeared to influence the work reported in this paper.

Data availability

Data will be made available on request.

Acknowledgments

Authors thank G. Zvejnieks and A. Platonenko for fruitful discussions. This study was supported by Eurofusion Enabling Research, European Union Project ENR-MAT.01. UT-T001-D001 "Investigation of defects and disorder in nonirradiated and irradiated Doped Diamond and Related Materials for fusion diagnostic applications (DDRM) — Theoretical and Experimental analysis". This work has been carried out within the framework of the EUROfusion Consortium, funded by the European Union via the Euratom Research and Training Programme (Grant Agreement No 101052200 — EUROfusion). Views and opinions expressed are however those of the author(s) only and do not necessarily reflect those of the European Union or the European Commission. Neither the European Union nor the European Commission can be held responsible for them. The research was performed in the Center of Excellence of the Institute of Solid State Physics, University of Latvia, supported through European Unions Horizon 2020 Framework Programme H2020-WIDESPREAD-01-2016-2017-TeamingPhase2 under grant agreement No. 739508, project CAMART2.

References

[1] N.E. Santos, F. Figueira, M. Neto, F.A.A. Paz, S.S. Braga, J.C. Mendes, Diamonds for life: developments in sensors for biomolecules, Appl. Sci. 12 (2022) 3000, https://doi.org/10.3390/app12063000.
[2] J.E. Field, The Properties of Natural and Synthetic Diamond, Academic Press, London, 1992.
[3] S. Szunerits, C.E. Nebel, R.J. Hamers, Surface functionalization and biological applications of CVD diamond, MRS Bull. 39 (2014) 517–524, https://doi.org/10.1557/mrs.2014.99.
[4] J. Raymakers, K. Haenen, W. Maes, Diamond surface functionalization: from gemstone to photoelectrochemical applications, J. Mater. Chem. C 7 (2019) 10134–10165, https://doi.org/10.1039/C9TC03381E.
[5] M. Nasladek, P. Pobedinskas, Recent advances in diamond science and technology: from quantum fundamentals to materials and applications, Phys. Status Solidi 220 (2023) 2300051, https://doi.org/10.1002/pssa.202300051.
[6] L.S. Pan, D.R. Kania, Diamond: Electronic Properties and Applications, Springer, New York, 1995.
[7] A.M. Zaitsev, Optical Properties of Diamond: A Data Handbook, Springer-Verlag, Berlin, 2001.
[8] J.V. Macpherson, A practical guide to using boron doped diamond in electrochemical research, Phys. Chem. Chem. Phys. 17 (2015) 2935–2949, https://doi.org/10.1039/C4CP04022H.
[9] N. Yang, S. Yu, J.V. Macpherson, Y. Einaga, H. Zhao, G. Zhao, G.M. Swain, X. Jiang, Conductive diamond: synthesis, properties, and electrochemical applications, Chem. Soc. Rev. 48 (2019) 157–204, https://doi.org/10.1039/C7CS00757D.
[10] O. Loto, M. Florentin, C. Masante, N. Donato, M.-L. Hicks, A.C. Pakpour-Tabrizi, R. B. Jackman, V. Zuerbig, P. Godignon, D. Eon, J. Pernot, F. Udrea, E. Gheeraert, Gate oxide electrical stability of p-type diamond MOS capacitors, IEEE Trans. Electron. Dev. 65 (2018) 3361–3364, https://doi.org/10.1109/TED.2018.2847340.
[11] Y.J. Lu, C.N. Lin, C.X. Shan, Optoelectronic diamond: growth, properties, and photodetection applications, Adv. Opt. Mater. 6 (2018) 1800359, https://doi.org/10.1002/adom.201800359.
[12] P. Siyushev, N. Nesladek, E. Bourgeois, M. Gulka, J. Hruby, T. Yamamoto, M. Trupke, T. Teraji, J. Isoya, F. Jelezko, Photoelectrical imaging and coherent spin-state readout of single nitrogen-vacancy centers in diamond, Science 363 (2019) 728–731, https://doi.org/10.1126/science.aav2789.
[13] Á. Gali, Ab initio theory of the nitrogen-vacancy center in diamond, Nanophotonics 8 (2019) 1907–1943, https://doi.org/10.1515/nanoph-2019-0154.
[14] F. Mazzocchi, G. Aiello, A. Meier, S. Schreck, P. Spaeh, D. Strauss, T. Scherer, Diamond window diagnostics for nuclear fusion applications — early concepts, EPJ Web Conf. 87 (2015) 04007, https://doi.org/10.1051/epjconf/20158704007.
[15] H. Yamada, A. Meier, F. Mazzocchi, S. Schreck, T. Scherer, Dielectric properties of single crystalline diamond wafers with large area at microwave wavelengths, Diamond Relat, Materials 58 (2015) 1–4, https://doi.org/10.1016/j.diamond.2015.05.004.
[16] F. Mazzocchi, S. Schreck, D. Strauss, G. Aiello, A. Meier, T. Scherer, Diamond windows diagnostics for fusion reactors — updates of the design, Fusion Eng. Des. 123 (2017) 820–824, https://doi.org/10.1016/j.fusengdes.2017.04.012.
[17] F.S. Gentile, F. Colasuonno, F. Pascale, K.E. El-Kelany, M. Causa, R. Dovesi, The VN_3 defect in diamond: a quantum mechanical simulation of the vibrational spectra and EPR properties, Carbon 170 (2020) 600–605, https://doi.org/10.1016/j.carbon.2020.08.050.
[18] F. Colasuonno, F.S. Gentile, W. Mackrodt, A.M. Ferrari, A. Platonenko, R. Dovesi, Interstitial defects in diamond: a quantum mechanical simulation of their EPR constants and vibrational spectra, J. Chem. Phys. 153 (2020) 024119, https://doi.org/10.1063/5.0014368.
[19] A.M. Ferrari, S. Salustro, F.S. Gentile, W.C. Mackrodt, R. Dovesi, Substitutional nitrogen in diamond: a quantum mechanical investigation of the electronic and spectroscopic properties, Carbon 134 (2018) 354–365, https://doi.org/10.1016/j.carbon.2018.03.091.
[20] G. Di Palma, B. Kirtman, F.S. Gentile, A. Platonenko, A.M. Ferrari, R. Dovesi, The VN_2 negatively charged defect in diamond. A quantum mechanical investigation of the EPR response, Carbon 159 (2020) 443–450, https://doi.org/10.1016/j.carbon.2019.12.031.
[21] L.L. Rusevich, E.A. Kotomin, A.I. Popov, G. Aiello, T.A. Scherer, A. Lushchik, The vibrational and dielectric properties of diamond with N impurities: first principles study, Diam. Relat. Mater. 130 (2022) 109399, https://doi.org/10.1016/j.diamond.2022.109399.
[22] J. Baima, A. Zelferino, P. Olivero, A. Erba, R. Dovesi, Raman spectroscopic features of the neutral vacancy in diamond from ab initio quantum mechanical calculations,

Phys. Chem. Chem. Phys. 18 (2016) 1961–1968, https://doi.org/10.1039/c5cp06672g.
[23] A. Zelferino, S. Salustro, J. Baima, V. Lacivita, R. Orlando, R. Dovesi, The electronic states of the neutral vacancy in diamond: a quantum mechanical approach, Theor. Chem. Acc. 135 (2016) 74, https://doi.org/10.1007/s00214-016-1813-0.
[24] J.C.A. Prentice, B. Monserrat, R.J. Needs, First principles study of the dynamic Jahn-Teller distortion on the neutral vacancy in diamond, Phys. Rev. B 95 (2017) 014108, https://doi.org/10.1103/PhysRevB.95.014108.
[25] D.E.P. Vanpoucke, K. Haenen, Revisiting the neutral C-vacancy in diamond: localization of electrons through DFT+U, Diam. Relat. Mater. 79 (2017) 60–69, https://doi.org/10.1016/j.diamond.2017.08.009.
[26] P. Deák, B. Aradi, M. Kaviani, T. Frauenheim, A. Gali, Formation of NV centers in diamond: a theoretical study based on calculated transitions and migration of nitrogen and vacancy related defects, Phys. Rev. B 89 (2014) 075203, https://doi.org/10.1103/PhysRevB.89.075203.
[27] L. Razinkovas, M.W. Doherty, N.B. Manson, C.G. Van de Walle, A. Alkauskas, Vibrational and vibronic structure of isolated point defects: the nitrogen-vacancy center in diamond, Phys. Rev. B 104 (2021) 045303, https://doi.org/10.1103/PhysRevB.104.045303.
[28] S. Salustro, G. Sansone, C.M. Zicovich-Wilson, Y. Noël, L. Maschio, R. Dovesi, The A-center defect in diamond: quantum mechanical characterization through the infrared spectrum, Phys. Chem. Chem. Phys. 19 (2017) 14478–14485, https://doi.org/10.1039/c7cp00093f.
[29] S. Salustro, F. Pascale, W.C. Mackrodt, C. Ravoux, A. Erba, R. Dovesi, Interstitial nitrogen atoms in diamond. A quantum mechanical investigation of its electronic and vibrational properties, Phys. Chem. Chem. Phys. 20 (2018) 16615–16624, https://doi.org/10.1039/c8cp02484g.
[30] S. Salustro, A. Erba, C.M. Zicovich-Wilson, Y. Noël, L. Maschioa, R. Dovesi, Infrared and Raman spectroscopic features of the self-interstitial defect in diamond from exact-exchange hybrid DFT calculations, Phys. Chem. Chem. Phys. 18 (2016) 21288–21295, https://doi.org/10.1039/c6cp02403c.
[31] A. Platonenko, D. Gryaznov, A.I. Popov, R. Dovesi, E.A. Kotomin, First principles calculations of the vibrational properties of single and dimer F-type centers in corundum crystals, J. Chem. Phys. 153 (2020) 134107, https://doi.org/10.1063/5.0023417.
[32] R. Dovesi, A. Erba, R. Orlando, C.M. Zicovich-Wilson, B. Civalleri, L. Maschio, M. Rerat, S. Casassa, J. Baima, S. Salustro, et al., Quantum-mechanical condensed matter simulations with CRYSTAL, Wiley Interdiscip. Rev. Comput. Mol. Sci. 8 (2018) e1360, https://doi.org/10.1002/wcms.1360.
[33] R. Dovesi, V.R. Saunders, C. Roetti, R. Orlando, C.M. Zicovich-Wilson, F. Pascale, B. Civalleri, K. Doll, N.M. Harrison, I.J. Bush, et al., CRYSTAL17 User's Manual, University of Torino, Torino, 2017.
[34] A.D. Becke, Density-functional thermochemistry. III. The role of exact exchange, J. Chem. Phys. 98 (1993) 5648–5652, https://doi.org/10.1063/1.464913.
[35] R. Dovesi, M. Causa, R. Orlando, C. Roetti, V.R. Saunders, Ab initio approach to molecular crystals: a periodic Hartree-Fock study of crystalline urea, J. Chem. Phys. 92 (1990) 7402–7411, https://doi.org/10.1063/1.458592.
[36] CRYSTAL Basis Sets Library. https://www.crystal.unito.it/basis_sets.html (accessed 25 February 2024)..
[37] G.J.B. Hurst, M. Dupuis, E. Clementi, Ab initio analytic polarizability, first and second hyperpolarizabilities of large conjugated organic molecules: applications to polyenes C_4H_6 to $C_{22}H_{24}$, J. Chem. Phys. 89 (1988) 385–395, https://doi.org/10.1063/1.455480.
[38] B. Kirtman, F.L. Gu, D.M. Bishop, Extension of the Genkin and Mednis Treatment for dynamic polarizabilities and hyperpolarizabilities of infinite periodic systems. I. Coupled perturbed Hartree–Fock theory, J. Chem. Phys. 113 (2000) 1294–1309, https://doi.org/10.1063/1.481907.
[39] R. Dovesi, B. Kirtman, L. Maschio, J. Maul, F. Pascale, M. Rérat, Calculation of the infrared intensity of crystalline systems. A comparison of three strategies based on Berry phase, Wannier function, and coupled-perturbed Kohn–Sham methods, J. Phys. Chem. C 123 (2019) 8336–8346, https://doi.org/10.1021/acs.jpcc.8b08902.
[40] L. Maschio, B. Kirtman, M. Rérat, R. Orlando, R. Dovesi, Ab initio analytical Raman intensities for periodic systems through a coupled perturbed Hartree-Fock/Kohn-Sham method in an atomic orbital basis. I. Theory, J. Chem. Phys. 139 (2013) 164101, https://doi.org/10.1063/1.4824442.
[41] L. Maschio, B. Kirtman, M. Rérat, R. Orlando, R. Dovesi, Ab initio analytical Raman intensities for periodic systems through a coupled perturbed Hartree-Fock/Kohn-Sham method in an atomic orbital basis. II. Validation and comparison with experiments, J. Chem. Phys. 139 (2013) 164102, https://doi.org/10.1063/1.4824443.
[42] R.A. Evarestov, D. Gryaznov, M. Arrigoni, E.A. Kotomin, A. Chesnokov, J. Maier, Use of site symmetry in supercell models of defective crystals: polarons in CeO_2, Phys. Chem. Chem. Phys. 19 (2017) 8340–8348, https://doi.org/10.1039/C6CP08582B.
[43] R.A. Evarestov, A. Platonenko, D. Gryaznov, YuF. Zhukovskii, E.A. Kotomin, First-principles calculations of oxygen interstitials in corundum: a site symmetry approach, Phys. Chem. Chem. Phys. 19 (2017) 25245–25251, https://doi.org/10.1039/C7CP04045H.
[44] H.O. Pierson, Handbook of Carbon, Graphite, Diamond and Fullerenes: Properties, Processing, and Applications, Noyes publications, Park Ridge, NJ, 1993.
[45] J.A. van Wyk, O.D. Tucker, M.E. Newton, J.M. Baker, G.S. Woods, P. Spear, Magnetic-resonance measurements on the $^5A_2$ excited state of the neutral vacancy in diamond, Phys. Rev. B 52 (1995) 12657–12667, https://doi.org/10.1103/physrevb.52.12657.
[46] D.N. Jamieson, S. Prawer, K.W. Nugent, S.P. Dooley, Cross-sectional Raman microscopy of MeV implanted diamond, Nucl. Instrum. Methods Phys. Res., Sect. B 106 (1995) 641–645, https://doi.org/10.1016/0168-583X(96)80036-X.
[47] J.O. Orwa, K.W. Nugent, D.N. Jamieson, S. Prawer, Raman investigation of damage caused by deep ion implantation in diamond, Phys. Rev. B 62 (2000) 5461–5472, https://doi.org/10.1103/PhysRevB.62.5461.
[48] S.L.Y. Chang, A.S. Barnard, C. Dwyer, C.B. Boothroyd, R.K. Hocking, E. Ōsawa, R. J. Nicholls, Counting vacancies and nitrogen-vacancy centers in detonation nanodiamond, Nanoscale 8 (2016) 10548–10552, https://doi.org/10.1039/C6NR01888B.
[49] J. Baker-Jarvis, S. Kim, The interaction of radio-frequency fields with dielectric materials at macroscopic to mesoscopic scales, J. Res. Nat. Instit. Stand. Technol. 117 (2012) 1–60, https://doi.org/10.6028/jres.117.001.
[50] I. Laszlo, M. Kertesz, B. Slepetz, Y. Gogotsi, Simulations of large multi-atom vacancies in diamond, Diam. Relat. Mater. 19 (2010) 1153–1162, https://doi.org/10.1016/j.diamond.2010.05.001.